Thin Solid Films 517 (2009) 2775–2780

Contents lists available at ScienceDirect

Thin Solid Films

journal homepage: www.elsevier.com/locate/tsf

Characterization of n-type and p-type semiconductor gas sensors based on NiO_x doped TiO_2 thin films

A. Wisitsoraat [a,*], A. Tuantranont [a], E. Comini [b], G. Sberveglieri [b], W. Wlodarski [c]

[a] National Electronics and Computer Technology Center, 112 Pahol Yothin Rd., Pathumthani Thailand
[b] SENSOR, INFM-CNR, University of Brescia Via Valotti 9, Brescia, Italy
[c] School of Electrical and Computer Engineering, RMIT University, GPO Box 2476V, Melbourne 3001, Victoria, Australia

ARTICLE INFO

Article history:
Received 3 December 2007
Received in revised form 13 October 2008
Accepted 23 October 2008
Available online 7 November 2008

Keywords:
Titanium dioxide
Nickel oxide
Semiconductor gas sensor
Thin films
X-ray diffraction
X-ray photoelectron spectroscopy
Electron beam evaporation

ABSTRACT

This work presents the development of n-type and p-type gas-sensitive materials from NiO_x doped TiO_2 thin films prepared by ion-assisted electron-beam evaporation. TiO_2 gas-sensing layers have been deposited over a wide range of NiO_x content (0–10 wt.%). The material analysis by atomic force microscopy, X-ray photoemission spectroscopy, and X-ray diffraction suggests that NiO_x doping does not significantly affect surface morphology and Ni element may be a substitutional dopant of the TiO_2 host material. Electrical characterization shows that NiO_x content as high as 10% wt. is needed to invert the n-type conductivity of TiO_2 into p-type conductivity. There are notable gas-sensing response differences between n-type and p-type NiO_x doped TiO_2 thin film. The responses toward all tested reducing gases tend to increase with operating temperature for the n-type TiO_2 films while the response decreases with temperature for p-type TiO_2 film. In addition, the p-type NiO_x doping results in the significant response enhancement toward tested reducing gases such as acetone and ethanol at low operating temperature of 300 °C.

1. Introduction

TiO_2 is a versatile material, which has been used in many applications such as gas sensor, solar cell, photocatalytic layer for self-cleaning glass, optical coating for filters and waveguides, etc. TiO_2 is one of the most promising gas-sensing materials due to its high temperature stability, harsh environment tolerance, and catalytic properties. For gas sensing applications, TiO_2 is used in anatase phase that has lower resistance and higher response to gas adsorbents than the rutile phase, which is stable at higher temperatures. TiO_2 nanocrystalline thin films were preferred because of their stable and good gas-sensing characteristics at operating temperatures below 400 °C.

However, its low electrical n-type conductivity inhibits its practical implementation as conductometric sensor. The addition of foreign atoms, such as Sn, Cr, Nb, W, Mo into TiO_2 host has been widely studied to improve its gas sensing behaviors [1–10]. Since the majority of these gas-sensitive layers are n-type semiconductors owing to intrinsic doping provided by preparation methodologies, p-type semiconductors sensitive to gases is lacking and it is now highly demanded for gas sensing applications such as sensor arrays for electronic nose because p-type semiconductor gas sensors would have much different gas-sensing pattern from n-type ones. For this reason, it is important to develop a simple way to produce a p-type semiconductor. Some p-type TiO_2 gas sensors, including Cr and W doped TiO_2, have been reported. However, these p-type TiO_2 gas sensors utilize rutile phase structure, which is formed by high post-deposition annealing temperature. The rutile phase TiO_2 is not desirable because it is less gas-sensitive and not stable at low operating temperatures.

Electron-beam (e-beam) evaporation is one of preferred techniques for thin film gas sensor fabrication because of ease of batch fabrication and ability to form high-quality multilayer thin film structures [11,12]. In addition, doping flexibility of this method presents an advantage over the sputtering process. For sputtering, doping may be done by means of insets or specially prepared alloyed targets. Low doping concentrations and uniform doping are difficult to achieve by the former method while the later one is considerably more expensive. With e-beam evaporation, uniform doping over a wide range of concentrations can be simply achieved by powder mixing of the source materials.

NiO_x is a gas sensing material with p-type conductivity [13,14]. However, NiO_x is not a promising gas sensing material because of its very high resistivity, long response/recovery time and poor long-term stability. NiO_x supported TiO_2 should be an interesting p-type metal oxide mixture. Recently, studies on fabrication and magnetic/photocatalytic properties of Ni doped TiO_2 thin films have been presented [15–18]. However, there have been very few studies on gas sensing behaviors of this kind of material. In this work, we systematically study NiO_x doped TiO_2 thin films prepared by ion-assisted electron-beam evaporation for gas sensing applications.

* Corresponding author. Tel.: +66 2 564 6900; fax: +66 2 564 6771.
E-mail address: anurat.wisitsoraat@nectec.or.th (A. Wisitsoraat).

0040-6090/$ – see front matter © 2008 Elsevier B.V. All rights reserved.
doi:10.1016/j.tsf.2008.10.090

2. Experimental details

2.1. Materials for gas sensor fabrication

The oxide materials used for the deposition are analytical grade (99.9%) TiO_2 and NiO_x powders. In this study, they were thoroughly mixed by the weight ratio of 0.9:0.1, 0.95:0.05, and 0.99:0.01, respectively. In addition, pure TiO_2 and NiO_x were also made as reference materials for comparison and analysis. The prepared materials are listed and labeled by material and composition codes as shown in Table 1. For e-beam evaporation, the mixed powder was compressed into cylindrical pellets. The substrates for thin film coating were 200 μm-thick alumina substrate. Platinum (Pt) is used as the inert material for sensor electrode and thin film heater.

2.2. Gas sensor fabrication

The gas sensor fabrication process started with the deposition of metal oxide thin film. Prior to deposition, the alumina substrates were cleaned by oxygen-ion bombardment in a vacuum pressure of $\sim 1.31 \times 10^{-2}$ Pa. This cleaning was performed to improve adhesion of the film to the substrates by removing moisture and any organic contaminants on the surface. The metal oxide layer was then e-beam evaporated under oxygen-ion beam with an oxygen flow of 25 sccm at a vacuum of 1.31×10^{-2} Pa. The oxygen ion beam was used to add oxygen atom into the film to compensate for oxygen decomposition from the evaporated metal oxide material. As a result, the metal oxide film would have sufficient oxygen throughout the film. Alumina substrate temperature, deposition rate, and film thickness were 200 °C, 2 Å/s, and 300 nm, respectively.

For this study, the depositions were conducted with different TiO_2–NiO_x compositions (Table 1). The films were then annealed inside a furnace under controlled flux of humid synthetic air at 500 °C. Next, Pt electrodes were sputtered over the metal oxide layer and substrate through interdigitated shadow masks. Finally, a Pt heater was deposited by sputtering on the backside through shadow masking. For electrical testing, the sensor electrodes and Pt heaters were gold-wire bonded for electrical connection to a package. The surface morphology, microstructure, and crystal structure of metal oxide thin films were examined by means of atomic force microscopy (AFM), scanning electron microscopy (SEM), X-ray photoemission spectroscopy (XPS), and X-ray diffraction (XRD).

AFM measurements (Seiko Instrument model SPI4000) were conducted in dynamic force mode operated at vibrational frequency of 292 kHz scanning over 5 μm × 5 μm area at a scanning rate of 1 Hz. The AFM tip was a commercial silicon tip with radius curvature of 10 nm, cone angle of 22° and tip height of ~10 μm and its cantilever beam is 130 μm long, 35 μm wide and ~2 μm thick. SEM measurements (Hitachi model S-3400N) were performed in secondary electron mode at an accelerating voltage of 20 kV. XPS measurements (In-house system developed at National Synchrotron Research Center, Thailand) were performed under an ultra-high vacuum condition at $\approx 10^{-8}$ Pa. Prior to XPS measurement, the metal oxide thin films on 3 × 3 mm^2 alumina substrates were in-situ cleaned to minimize carbon contamination by sputtering with 1 keV Argon beam at vacuum of 10^{-5} Pa.

In XPS measurement, a 2 mm monochromatized X-ray beam (Mg $K_{\alpha 1}$ with wavelength of 83.4 nm) was then incident on a sample at 45° to normal and a hemispherical electron energy analyzer with multi-channeltron detector (Thermo Scientific model Alpha 110) probed photoelectrons at the normal axis. The binding energy and scattering factor calibration were obtained from Avantage data system software provided by Thermo VG Scientific. In addition, the effect of binding energy shifts due to charging on insulating alumina substrate has been corrected by comparing the energy of the same film that is simultaneously deposited on a conductive silicon substrate. XRD measurements (Bruker D8 Advanced XRD system) were conducted in the standard variable angle diffraction mode at a scanning rate of 0.3°/min using a rotating anode X-ray generator operated at 40 kV/35 mA, which produced Cu $K_{\alpha 1}$ radiation line (wavelength = 0.154 nm).

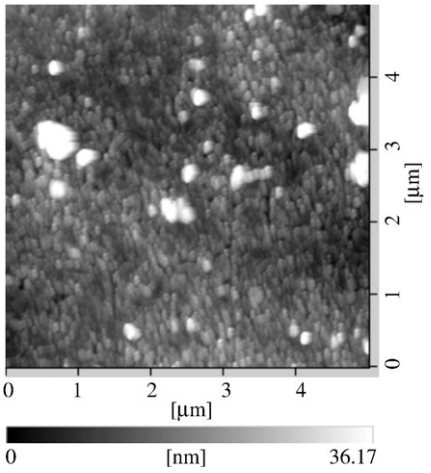

Fig. 1. 2D AFM image of e-beam evaporated 10% at. NiO_x–TiO_2 thin film after annealing.

2.3. Gas sensing measurements

The gas-sensing characteristics of metal oxide thin films were characterized toward Ethanol, Acetone, Ammonia, CO and NO_2. The flow through technique was used to test the gas-sensing properties of thin films. A constant flux of synthetic air of 0.5 l/min was as gas carrier into which the desired concentration of pollutants–dispersed in synthetic air–was mixed. All measurements were conducted in a temperature-stabilized sealed chamber at 20 °C under controlled relative humidity of 40%. The Pt-heater was heated by a regulated direct (dc) power supply to different operating temperatures. The operating temperature was varied from 200 ° C to 500 °C. The resistances of various sensors were continuously monitored with a computer-controlled system by voltage-amperometric technique with 1 V dc bias and current measurement through a picoammeter. The sensor was exposed to a gas sample for 20 min for each gas concentration and then the air flux was restored for 20 min.

Table 1
Elemental composition and structural parameters of NiO_x doped TiO_2 thin films prepared with different source materials obtained from XPS and XRD analyses

Source materials	TiO_2 (wt.%)	100	99	95	90	0
	NiO_x (wt.%)	0	1	5	10	100
Elemental composition (at.%)	Ti	28	26	25	22	–
	Ni	–	0.8	3	7	45
	O	77	73	72	71	55
	O:(Ti+Ni)	2.7	2.7	2.6	2.4	1.2
Ni oxidation state (at.%)	Ni^{+2}	–	52	54	56	61
	Ni^{+3}	–	32	32	33	35
	Ni^{+4}	–	16	14	11	4
Average Ni oxidation state		–	2.64	2.60	2.53	2.44
Crystal structure	Lattice constant (Å)	3.54	3.54	3.55	3.56	2.41
	Average crystallite size (nm)	11.86	11.62	11.24	10.88	21.81

3. Experimental results

3.1. Structural characteristics

Typical atomic force micrograph (AFM) of 10% NiO_x doped TiO_2 thin film is shown in Fig. 1. AFM images suggest that e-beam

evaporated metal oxide thin films have typical polycrystalline structure with some relatively large grains scattered over fine grain majority. The grain size estimated by AFM analysis software is in the range between 10 nm and 30 nm. There is no significant morphological difference between TiO_2 thin films with different NiO_x contents.

The information on the elemental composition of the doped oxide thin films is characterized by XPS measurement. The full XPS spectra taken from Ni doped TiO_2 thin films confirm the presence of Ti, Ni, and O elements. The atomic contents of Ti, Ni, and O in the thin film have been calculated based on library standard and listed in Table 1. The content of natural carbon contamination was confirmed to be very small (<0.2%) and thus it is ignored in the composition determination. It can be seen that the atomic contents of Ti:Ni in the thin film is in accordance with the content of the source materials prepared from powder mixing. In addition, the oxygen content tends to decrease as the Ni content increases. This suggests that the corresponding oxygen vacancies on the film increase as the Ni content increases. The XPS spectra of Ni element of NiO_x–TiO_2 thin films are shown in Fig. 2. The spectra consist of two groups of peaks. $Ni2p^{3/2}$ group is located in the range between 850 and 865 eV while $Ni2p^{1/2}$ group is located in the range between 868 and 885 eV. It is evident that the peak is increased in magnitude and shifted toward higher binding energy as the Ni content increases.

The oxidation state of each metallic element can be determined by the modeling of XPS peaks. The XPS spectra are fitted and deconvoluted by Gaussian curves corresponding to peaks of various oxidation states of Ni element from $Ni2p^{3/2}$ group as illustrated in the inset of Fig. 2. In this energy range, it can be seen that XPS spectra can be decomposed into three Gaussian curves, which should be corresponding to three different oxidation states of Ni ions that can be identified as Ni^{+2}(NiO) at ~854.5 eV, Ni^{+3}(Ni_3O_2) at ~857.8 eV, and Ni^{+4} (NiO_2) at ~861.2 eV respectively [19–21]. The relative content of oxidation states and average oxidation state of Ni element are estimated and listed in Table 1. It can be seen that the contents of high oxidation state (Ni^{+3} and Ni^{+4}) decrease as the NiO_x content increases. Thus, the average oxidation state of Ni decreases as Ni content increases and the oxidation state of NiO_x doped TiO_2 thin film is higher than that of pure NiO_x thin film. The change of relative content of oxidation state suggests interaction between Ni and other elements, which may be in the form of substitutional doping. This XPS result can not be compared to some other recent work because XPS

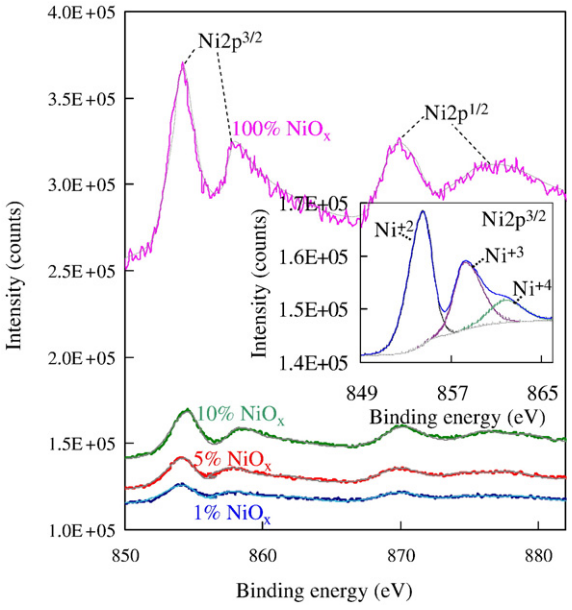

Fig. 2. XPS spectra for Ni element of e-beam evaporated NiO_x–TiO_2 thin film after annealing.

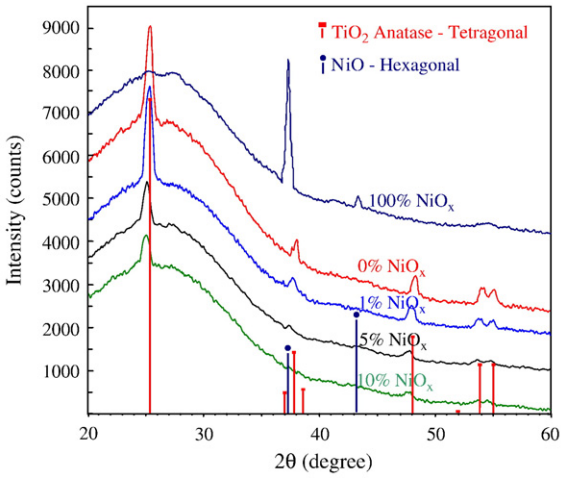

Fig. 3. XRD patterns of e-beam evaporated NiO_x–TiO_2 thin film after annealing.

spectra of Ni element for Ni doped TiO_2 thin films were not reported [22,23].

The information on the crystal structure of the doped oxide thin films is revealed in X-ray diffractogram (XRD) as shown in Fig. 3. The patterns of samples with different NiO_x contents only contain anatase: tetragonal peaks of TiO_2 at 25.8°, 38.2°, 48.5°, and 54.2°. However, the peaks are broader and reduced in magnitude as NiO_x content increases. In addition, the locations of peaks are shifted toward smaller angle. The maximum peak shift of the sample prepared with 10% NiO_x is measured to be 0.38°. The effect of peak shift is corresponding to the change of lattice constant of the crystal structure. The lattice constants of the films with different NiO_x contents have been calculated from Brag's law and listed in Table 1. It can be seen that the lattice constant is increased from ~3.54 Å to ~3.56 Å or about 0.5% change as the NiO_x contents increases from 0% to 10%. Although the lattice constant can not be calculated with high precision because the XRD peaks are not very sharp, the estimated lattice constant may be used to suggest lattice modification possibly due to substitutional doping effect.

Comparing to pure the diffractogram of NiO_x thin film, it can be seen that expected hexagonal NiO_2: peaks at 37.3° and 43.3° can not be identified in NiO_x doped TiO_2 thin films. These indirectly indicate that NiO_x component is soluted in the TiO_2 host as a substitutional dopant rather than a secondary phase oxide. The observed XRD result is similar to other studies on Ni doped TiO_2 thin films [15,22], which suggested that Ni is a substitutional dopant of TiO_2 lattice. Furthermore, the additional observation from XPS analysis that amount of oxygen vacancies increases with Ni content further suggests that Ni should substitute Ti in the crystal (Each Ni (charged +2) substitution on Ti (charged +4) induces a single oxygen vacancy (charged +2) due to charge conservation). However, NiO secondary phase with very small grains may exist and its existence could not be revealed by XRD and XPS. Thus, additional structural characterization will be performed by transmission electron microscopy (TEM) and extended X-ray absorption fine structure spectroscopy (EXAFS) to clarify the exact structure of Ni element in the TiO_2 thin film. The additional characterizations are currently in progress and the results will be reported elsewhere.

The effect of NiO_x content on crystallite size has also been evaluated from XRD data. The crystallite sizes of the films with different NiO_x contents have been calculated from Scherrer's equation and listed in Table 1. It is noticed that the grain size is decreased from 11.67 nm to 10.88 nm, about 0.9% change as the NiO_x contents increases to from 1% to 10%. The change in grain size is very small and thus it can not be observed by AFM or SEM characterization. However, the calculated grain size from XRD is in the same order as observed by AFM.

3.2. Gas-sensing characteristics

The semiconductor sensing properties are based on reactions between semiconductor and gases in the atmosphere, which produce a change in the semiconductor resistance. The reaction that leads to a change in the conductivity is adsorption of gases at surface. Initially, oxygen in the atmosphere adsorbs and extracts electrons from the conduction band of the semiconductor. When the desired concentration of gases is introduced, many possible processes can occur. The gases may react with the oxygen adsorbed on the surface or with the semiconductor surface, or with both; for an n-type semiconductor the resistivity increases due to electron capture by an oxidizing gas and decreases with the presence of a reducing gas owing to electron transfer into the conduction band, while the opposite holds for a p-type semiconductor. Discrimination between the many possible processes involved is very difficult from the theoretical point of view.

The gas sensing properties are characterized in term of dynamic change of resistance and gas-sensing response. The gas sensing response of n-type semiconductor based conductometric gas sensor to a reducing gas is normally defined as the ratio, $\Delta R/R_g$, of the resistance change (ΔR) due to gas introduction to the resistance when the gas is present (R_g) while the response to an oxidizing gas is defined as the ratio, $\Delta R/R_0$, of the resistance change to the resistance in air (R_0). For p-type semiconductor gas sensor, the definitions are reversed. The gas-sensing response was calculated from dynamic variation of the conductance due to gas pulses introduction and plotted versus various parameters including temperature and gas concentration.

Fig. 4 illustrates the dynamic response to acetone of TiO_2 thin films with different NiO_x contents. It can be seen that the resistances of the TiO_2 thin film with 1% and 0% NiO_x are reduced upon the exposure to reducing gas, indicating the n-type semiconductor behavior and the behavior of 1% NiO_x is not considerably different from the undoped one. On the other hand, the resistances of the TiO_2 thin film with 10% NiO_x and pure NiO_x thin film are increased upon the exposure to reducing gas, signifying a p-type semiconductor behavior. Thus, the presence of nickel oxide in the thin film causes an inversion the electrical properties of the TiO_2 semiconductor leading to a p-type sensing behavior when the NiO_x content reaches 10%. Comparing to the pure NiO_x thin film, it is evident that the p-type TiO_2 thin film has much higher gas sensing response with shorter response and recovery time. In addition, the p-type TiO_2 based thin film exhibit much less base line drift that than the pure NiO_x thin film. Moreover, it can be seen that the resistance of TiO_2 thin films increase by more than 3 order of magnitude due to the presence of nickel element as the NiO_x content increases from 0% to 10%.

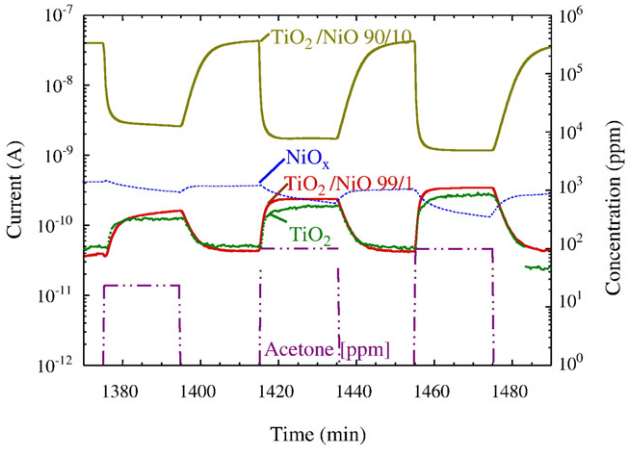

Fig. 4. Variation of the current flowing through NiO_x–TiO_2 thin films as acetone square pulses are introduced in the test chamber at an operating temperature of 300 °C and with 40%RH.

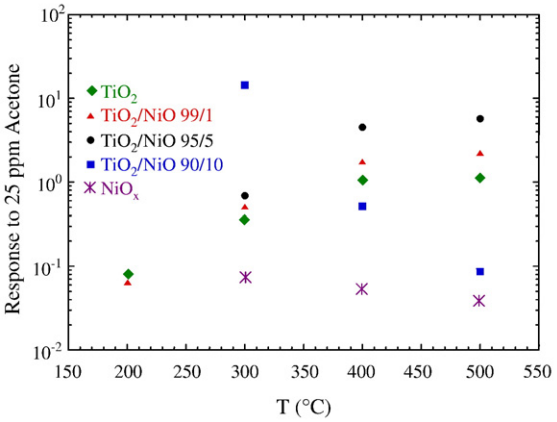

Fig. 5. Acetone response of NiO_x–TiO_2 thin films versus operating temperature for a concentration of 25 ppm.

The calculated responses toward acetone at 25 ppm concentration versus operating temperature of TiO_2/NiO_x thin films are reported in Fig. 5. It can be seen that the response toward acetone is improved compared to undoped one as NiO_x content increases. In addition, the response tends to increase with operating temperature when the TiO_2 thin films still behave as n-type semiconductor. On the contrary, the response decreases with operating temperature when the TiO_2 films become p-type semiconductor. Nevertheless, p-type NiO_x doping results in significant acetone response enhancement of more than one order of magnitude at operating temperature of 300 °C. Moreover, the p-type NiO_x doped TiO_2 thin film has higher response to acetone than the pure NiO_x thin film by more than two orders of magnitude at operating temperature of 300 °C.

Fig. 6 shows the selected dynamic responses toward ethanol of TiO_2/NiO thin films with 0%, 1% 5% and 100% NiO_x content. It can be seen that the sample with 5% and 1% NiO_x contents still behave as n-type semiconductors, but with lower conductivity than undoped TiO_2, a possible indication of doping compensation. In addition, the response toward ethanol is increased compared to undoped one as NiO_x content increases. In contrast, pure NiO_x thin film shows a p-type semiconductor sensing behavior but with relatively low and slow response. The calculated responses toward ethanol at 100 ppm concentration versus operating temperature of TiO_2/NiO_x thin films are shown in Fig. 7. It can be noticed that the NiO_x doping results in a response improvement toward ethanol compared to undoped one and

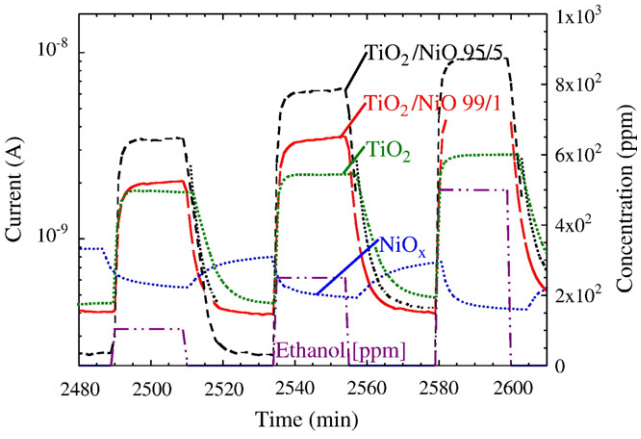

Fig. 6. Variation of the current flowing through NiO_x–TiO_2 thin films as ethanol square pulses are introduced in the test chamber at an operating temperature of 400 °C and with 40%RH.

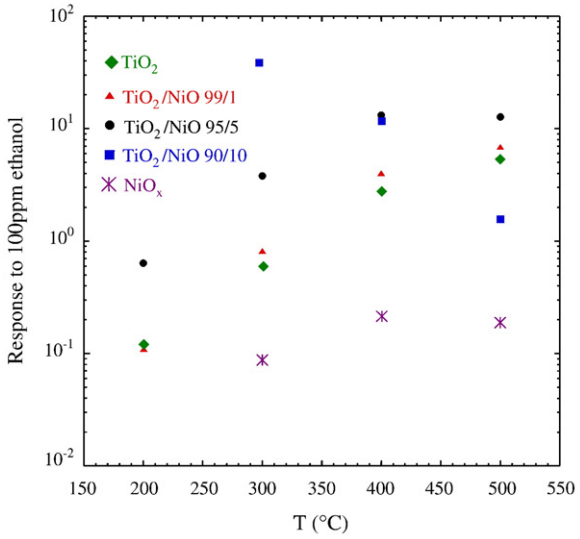

Fig. 7. Ethanol response of NiO_x–TiO_2 thin films versus operating temperature for a concentration of 100 ppm.

the response tends to increase with operating temperature when TiO_2 films still behave as n-type semiconductor. Similar to the acetone case, the ethanol response decreases with operating temperature when the TiO_2 films becomes p-type semiconductor and p-type NiO_x doping results in significant ethanol response enhancement at low operating temperature of 300 °C. In addition, the p-type NiO_x doped TiO_2 thin film shows higher response to ethanol than the pure NiO_x thin film by almost three orders of magnitude at operating temperature of 300 °C.

The responses toward ammonia at 2 ppm concentration versus operating temperature of TiO_2/NiO thin films are shown in Fig. 8. It can also be seen that the NiO_x doping results in response improvement behaviors similar to acetone and ethanol cases. However the response of n-type TiO_2 thin film is very small and almost negligible compared to the two previous cases. Similar to other cases, the ammonia response decreases with operating temperature when the TiO_2 films becomes p-type semiconductor and p-type NiO_x doping results in significant ammonia response enhancement at low operating temperature of 300 °C. Moreover, the p-type NiO_x doped TiO_2 thin film exhibits much higher response to ammonia than the pure NiO_x thin film at operating temperature of 300–400 °C.

The responses toward CO at 500 ppm concentration versus operating temperature of TiO_2/NiO_x thin films are shown in Fig. 9. It can be seen that the NiO_x doping seems not to influence in the response toward CO and the response is very low and independent of

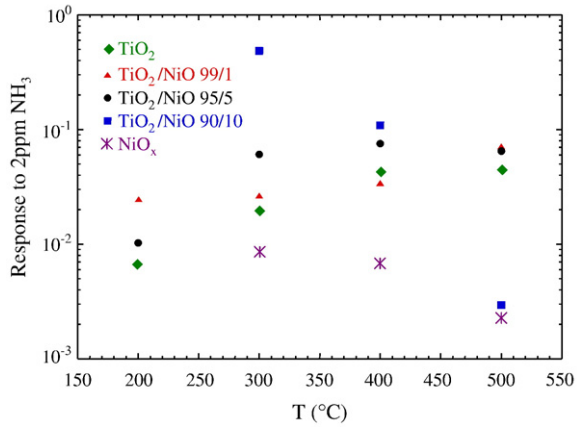

Fig. 8. Ammonia response of NiO_x–TiO_2 thin films versus operating temperature for a concentration of 2 ppm.

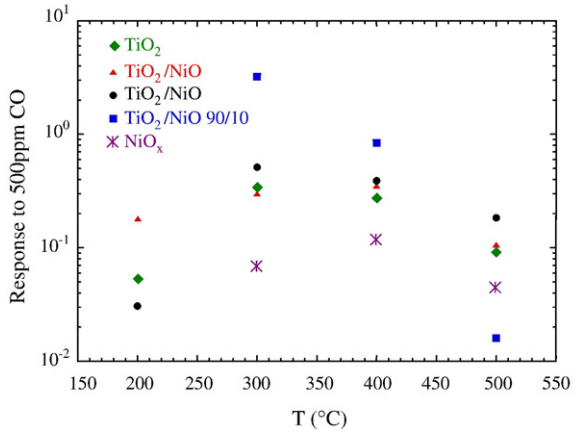

Fig. 9. CO response of NiO_x–TiO_2 thin films versus operating temperature for a concentration of 500 ppm.

operating temperature for the n-type TiO_2 thin films. Also similar to other cases, the CO response decreases with operating temperature when the TiO_2 films becomes p-type semiconductor and p-type NiO_x doping results in significant CO response enhancement at low operating temperature of 300 °C. Likewise, the p-type NiO_x doped TiO_2 thin film shows higher response to CO than the pure NiO_x thin film at operating temperature of 300–400 °C.

The calculated responses toward NO_2 at 1 ppm concentration versus operating temperature of TiO_2/NiO thin films are shown in Fig. 10. It can be seen that the NiO_x doping seems not to influence in the response toward NO_2 and the response is very low and decreases with operating temperature for all TiO_2 thin films. Unlike other cases, p-type NiO_x doping does not result in significant NO_2 response enhancement at low operating temperature. However, the p-type NiO_x doped TiO_2 thin film still has higher response to NO_2 than the pure NiO_x thin film at operating temperature of 300 °C.

Since according to AFM, XPS, and XRD analysis NiO_x doping does not notably affect the morphological structure of the TiO_2 thin films, the gas-sensing behaviors of NiO_x doped TiO_2 thin films should be mainly attributed to chemical and catalytic properties of nickel elements The enhancement of response toward acetone, ethanol, ammonia, and CO may be due to enhanced chemical reaction by nickel on the surface because it is known that nickel is a catalyst for hydrogen and hydrocarbon gases commonly used in the anode of solid oxide fuel cell. Nevertheless, further study still needs to be done to understand the detailed gas-sensing mechanisms of the NiO_x doped TiO_2 thin film.

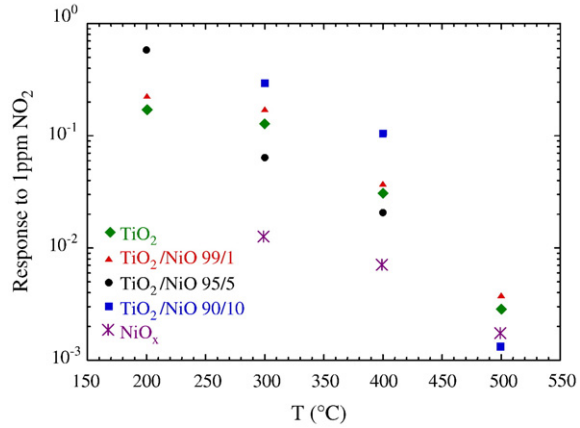

Fig. 10. NO_2 response of NiO_x–TiO_2 thin films versus operating temperature for a concentration of 1 ppm.

4. Conclusion

In conclusion, we have developed a p-type gas-sensitive material using NiO_x doped TiO_2 thin film prepared by ion-assisted electron-beam evaporation. TiO_2 gas-sensing layers have been deposited over a wide range of NiO_x content (0–10 wt.%). The materials have been structurally characterized by means of AFM and XRD in order to correlate physical properties with gas sensing behaviors. The analysis results suggest that NiO_x doping does not significantly affect surface morphology and Ni element should be a substitutional dopant of TiO_2 host material. Electrical characterization shows that NiO_x content as high as 10% wt. is needed to invert the n-type conductivity of TiO_2 into p-type conductivity. There are notable differences between n-type and p-type NiO_x doped TiO_2 thin film. The responses toward all tested reducing gases tend to increase with operating temperature for the n-type TiO_2 films while the response decreases with temperature for p-type TiO_2 film. In addition, the p-type NiO_x doping results in the significant response enhancement toward tested reducing gases such as acetone and ethanol at low operating temperature of 300 °C. Moreover, the p-type NiO_x doped TiO_2 thin film exhibits much higher response all tested gases than the pure NiO_x thin film at operating temperature of 300–400 °C.

Acknowledgements

The authors would like to acknowledge the funding and the use of XPS system of National Synchrotron Research Center, Thailand. We would also like to appreciate an additional research fund from sensor program, National Electronics and Computer Technology Center, Thailand.

References

[1] E. Comini, V. Guidi, M. Ferroni, G. Sberveglieri, Sens. Actuators B100 (2004) 41.
[2] E. Comini, G. Sberveglieri, V. Guidi, Sens. Actuators B70 (2000) 108.
[3] K. Galatsis, Y.X. Li, W. Wlodarski, E. Comini, G. Sberveglieri, C. Cantalini, S. Santucci, M. Passacantando, Sens. Actuators B83 (2002) 276.
[4] M. Ferroni, V. Guidi, G. Martinelli, E. Comini, G. Sberveglieri, D. Boscarino, G. Della, J. Appl. Phys. 88 (2000) 1097.
[5] M. Ferroni, V. Guidi, G. Martinelli, P. Nelli, G. Sberveglieri, Sens. Actuators B44 (1997) 499.
[6] M. Gerlicha, S. Kornely, M. Fleischer, H. Meixner, R. Kassing, Sens. Actuators B83 (2003) 503.
[7] Y. Yamada, Y. Seno, Y. Masuoka, T. Nakamura, K. Yamashita, Sens. Actuators B66 (2000) 164.
[8] K. Zakrzewska, M. Radecka, M. Rekas, Thin Solid Films 310 (1997) 161.
[9] A. Ruiz, G. Dezanneau, J. Arbiol, A. Cornet, J.R. Morante, Thin Solid Films 436 (2003) 90.
[10] T. Oyabu, J. Appl. Phys. 53 (1981) 2785.
[11] H. Madhusudhana, N. Chanodrkar, Sens. Actuators B9 (1992) 1.
[12] S. Shukla, S. Seal, L. Ludwig, C. Parish, Sens. Actuators B97 (2004) 256.
[13] I. Hotovy, J. Huran, P. Siciliano, S. Capone, L. Spiess, V. Rhacek, Sens. Actuators B70 (2001) 126.
[14] I. Hotovy, J. Huran, P. Siciliano, S. Capone, L. Spiess, V. Rhacek, Sens. Actuators B103 (2004) 300.
[15] N.H. Hong, J. Sakaib, W. Prellier, J. Magn. Magn. Mater. 281 (2004) 347.
[16] N.H. Hong, W. Prellier, J. Sakai, A. Hassini, Appl. Phys. Lett. 84 (2004) 2850.
[17] K.-S. Hwanga, J.-H. Jeonga, J.-H. Ahna, B.-H. Kim, Ceram. Int. 32 (2006) 935.
[18] D.L. Hou, H.J. Meng, L.Y. Jia, X.J. Ye, H.J. Zhou, X.L. Li, Phys. Lett. A364 (2007) 318.
[19] P.F. Luo, T. Kuwana, D.K. Paul, Peter M.A. Sherwood, Anal. Chem. 68 (1996) 3330.
[20] St.G. Christoskova, N. Danova, M. Georgieva, O.K. Argirov, D. Mehandzhiev, Appl. Catal., A Gen. 128 (1995) 219.
[21] V.Y. Young, F.C. Chang, K.L. Cheng, Appl. Spectrosc. 41 (1987) 994.
[22] Marshal Dhayal, S.D. Sharma, Chander Kant, K.K. Saini, S.C. Jain, Surf. Sci. 602 (2008) 1149.
[23] C. Parlog, M. Gartner, P. Osiceanu, V. Teodorescu, F. Moise, A. Ianculescu, Ceram. Int. 22 (1996) 95.